Three-dimensional calculations for a 4 kA, 3.5 MV, 2 microsecond injector with asymmetric power feed

Thomas P. Hughes and Robert E. Clark
Mission Research Corporation, 1720 Randolph, SE, Albuquerque, New Mexico 87106

Simon S. Yu
Lawrence Berkeley National Laboratory, 1 Cyclotron Road, Berkeley, California 94720
(Received 30 June 1999; published 15 November 1999)

The DARHT-2 accelerator under construction at Los Alamos National Laboratory requires a long flattop (2 μs) 2–4 kA, 3.5 MV, low-emittance electron beam source. The injector is being constructed at Lawrence Berkeley National Laboratory and consists of a large-area thermionic cathode mounted atop a vertical column. The 90° bend between the horizontally emitted beam and the column produces dipole and higher-pole fields which must be corrected. In addition, the fast rise of the current flowing into the vacuum tank excites rf modes which cause transverse oscillations of the beam centroid. We have modeled these effects with the 3D electromagnetic code LSP. The code has models for pulsed power transmission lines, space-charge-limited emission and transport of charged particles, externally applied magnetic fields, and frequency-dependent absorption of rf. We calculate the transverse displacement of the beam as a function of time during the current pulse, and the positioning and thickness of ferrite absorber needed to damp the rf modes. The numerical results are compared to analytic calculations.

PACS numbers: 29.27.–a, 41.85.Ja, 52.65.Rr

I. INTRODUCTION

The DARHT radiographic facility at LANL requires two linear induction accelerators at right angles to each other [1]. The second accelerator is currently being designed and will provide a long-pulse (2 μs flattop) high current (2–4 kA) beam. This paper describes calculations carried out for the beam injector, shown in Fig. 1. The thermionic emitter (about 9 cm in radius) is mounted on top of a vertical high-voltage conductor and insulator column inside a large vacuum vessel. This arrangement simplifies the problem of supporting the weight of the long insulator column. The diode is driven directly by a Marx bank which sits underneath the vacuum vessel. In order to produce a linear potential drop across the insulator column, resistors are wound helically around the insulator column, connecting the cathode dome on top to ground at the bottom. The beam is extracted at right angles to the high-voltage feed, and this results in both quasistatic and rf transverse forces on the beam. To calculate these effects, we have used the parallelized 3D electromagnetic particle-in-cell code LSP [2].

II. QUASISTATIC PERTURBATIONS

The largest perturbation to the beam is due to the transverse magnetic field produced in the anode-cathode (AK) gap by the current flowing in the vertical high-voltage conductor and the return currents flowing in the outer wall. The force is analogous to the hoop stress in an electron-beam ring, and deflects the beam upward in Fig. 1. If we neglect wall currents, the Biot-Savart law applied to the net current $I_{\rm net}$ (high-voltage conductor current less the resistor current) gives

$$B_\perp \approx \frac{\mu_0 I_{\rm net}}{4\pi R_{\rm AK}} \tag{1}$$

in the AK gap, where $R_{\rm AK}$ is the radius of the AK gap (the x coordinate in Fig. 1). For $I_{\rm net} = 4$ kA, $R_{\rm AK} = 1.35$ m, this gives about 3 G. The resulting deflection of the beam is given roughly by $\frac{1}{2}(eB_\perp/\gamma m_e c)d^2$ [where d is the AK gap length ($\approx$30 cm) and γ is the average relativistic factor in the gap], which is of the order of a few mm at the anode. In order to include the effect of wall currents, and obtain time-dependent effects, we carried out a calculation through the approximately 500 ns rise time of the voltage pulse using LSP. In this calculation, the Marx bank is approximated using a simple 745 Ω transmission line (matched to the nominal 875 Ω diode impedance in parallel with a 5 kΩ resistor) connected to the coaxial conductors at the bottom of Fig. 1. The numerical grid dimension is about 3 cm and the time step is the electromagnetic Courant-condition value. The 5 kΩ resistor is represented by a cylindrical shell of finite conductivity just inside the insulator. The current and voltage at the inlet (the bottom of Fig. 1) and the beam current and AK voltage are shown in Fig. 2. The difference between the steady-state inlet current and the beam current flows in the 5 kΩ resistor. A vector plot of return currents in the cylindrical part of the vacuum vessel wall is shown in Fig. 3. The effect of the asymmetry of the wall return currents on the azimuthal magnetic field is shown in Fig. 4, where we see that there is a strong azimuthal asymmetry at the elevation of the AK gap.

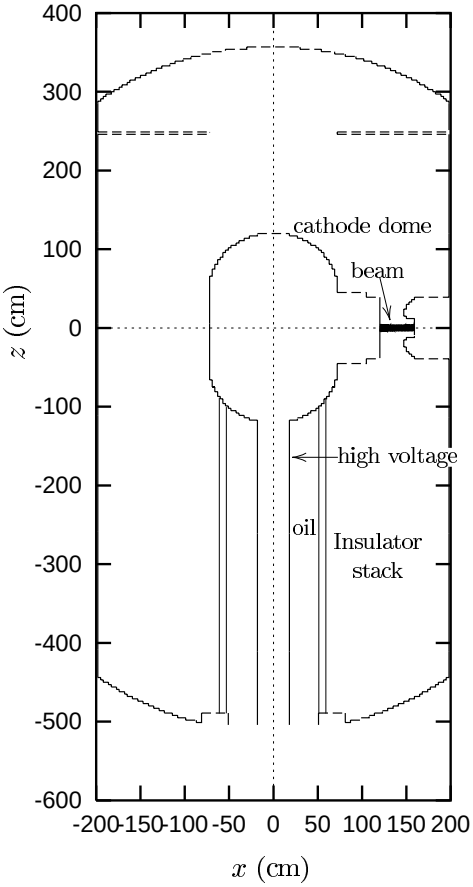

FIG. 1. Injector geometry used in 3D simulations.

The transverse magnetic field in the AK gap and the beam deflection 30 cm from the cathode (the AK gap is about 30 cm) are plotted in Fig. 5. In this simulation, no external focusing fields are applied. In practice, the anode contains solenoidal magnets to capture the high-current beam. To compensate for the transverse magnetic field in the AK gap, static dipole coils wound on the solenoidal magnets will be used to steer the beam back

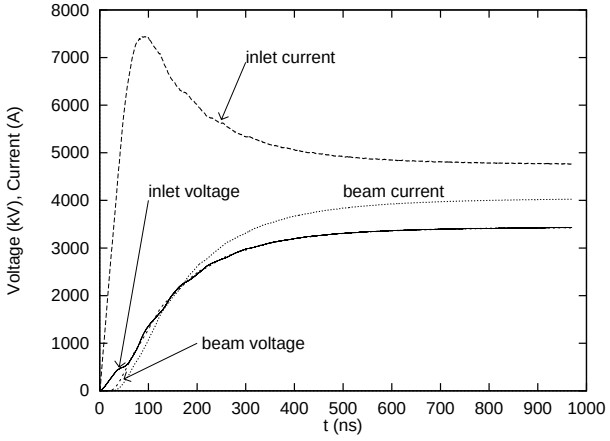

FIG. 2. Inlet and AK current and voltage vs time.

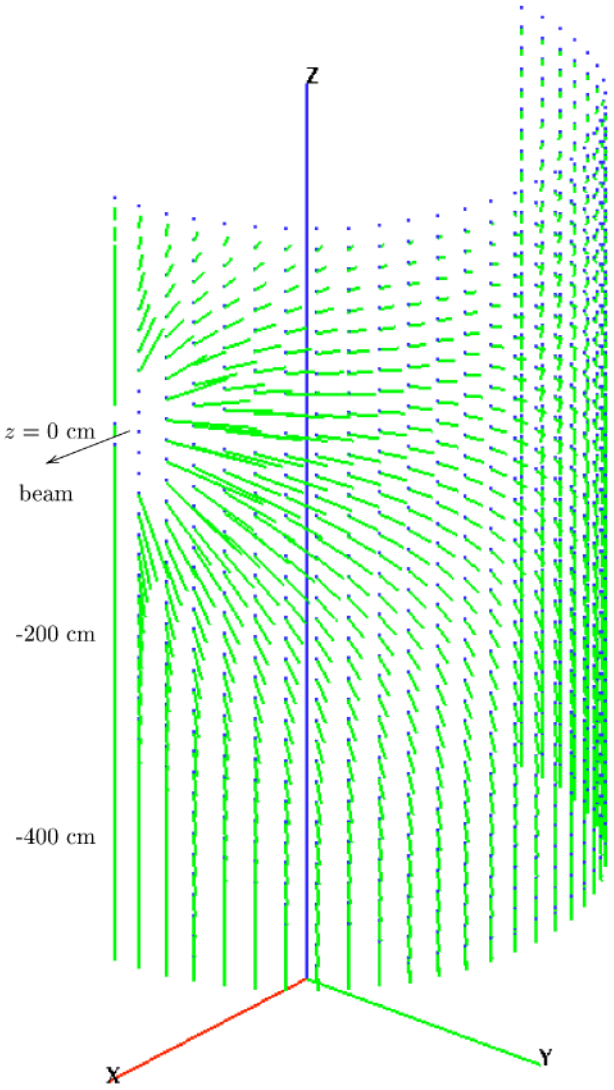

FIG. 3. (Color) Vector plot of surface currents flowing in the wall of the injector vessel.

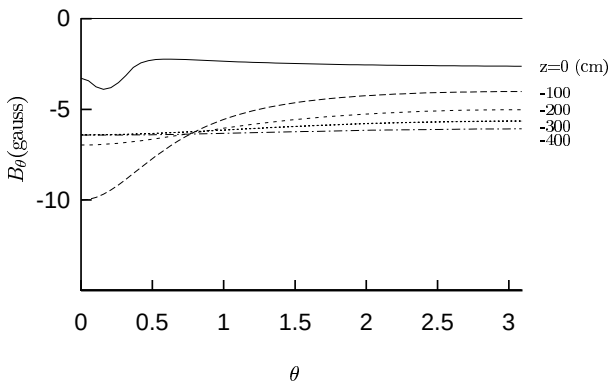

FIG. 4. Azimuthal variation of B_θ at different z positions (in cm), at a radius of 134 cm. The AK gap is at $\theta = 0$, $z = 0$.

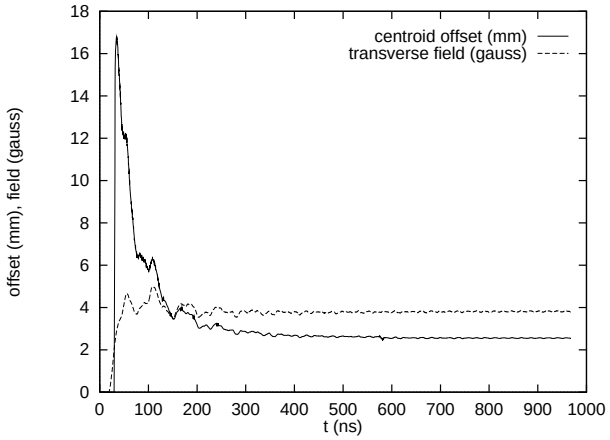

FIG. 5. Transverse magnet field 14 cm from the cathode and beam deflection 30 cm from the cathode.

on axis. If the deflecting field were proportional to the beam current, as would be the case if the system had a matched impedance from the Marx to the AK gap, then the correction fields would need to vary with the beam current to keep the beam head on axis. However, because of the large capacitance of the vacuum vessel (about 320 pF), the rise time of the current flowing into the vacuum vessel is much shorter than the rise time of the beam current (see Fig. 2). It turns out that the deflecting field in the AK gap is almost constant during the rise of the beam current, as shown in Fig. 5. As a result, static correction fields provide much better steering for the beam head than one might expect.

One option considered for reducing the asymmetry of the diode injector was to lengthen the cathode stalk and create a cylindrically symmetric wall around it, as shown in Fig. 6. The outer wall radius of about 1 m was constrained by the requirement of keeping the field stress on the stalk surface to less than about 100 kV/cm. The transverse magnetic field in the AK gap drops as a function of the length of the stalk, as shown in Fig. 7. An extension of almost 2 m is required to reduce the centroid offset by an order of magnitude. The added cost of implementing this scheme did not seem to be justifiable.

In Fig. 1, the high-voltage conductor and the cathode dome are shown as a single surface. In practice, they will be separate conductors connected by current straps. A coarse-grained diagram of how current flows on the surface of the cathode dome to the emission surface is shown in Fig. 8. On the cathode stalk, the difference between the current flowing in the top and bottom halves is about 740 A for a 4 kA beam current. This asymmetry is consistent with a simplified calculation of the dipole current on the surface of a conducting cylinder immersed in a transverse magnetic field (see Fig. 9). The magnetic scalar potential Ψ satisfies

$$\frac{1}{r}\frac{\partial}{\partial r}\,r\,\frac{\partial \Psi}{\partial r} + \frac{1}{r^2}\,\frac{\partial^2 \Psi}{\partial \theta^2} = 0\,. \qquad (2)$$

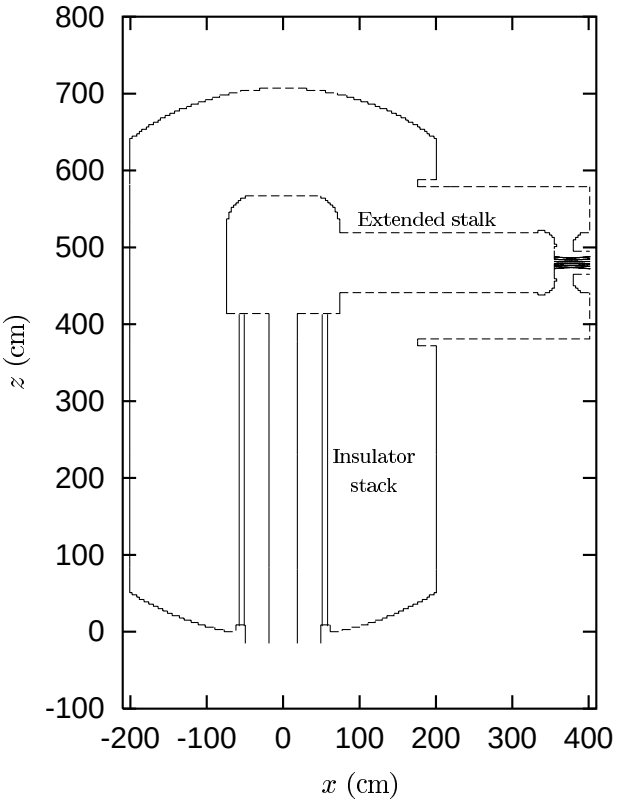

FIG. 6. Extended cathode stalk to reduce diode asymmetry (based on an earlier design than that in Fig. 1).

The general solution is

$$\Psi(r,\theta) = \sum_{l=-\infty}^{l=\infty} (A_l r^l + B_l r^{-l}) e^{il\theta} + \text{c.c.} \qquad (3)$$

Applying the boundary conditions at $r = a$ ($B_\perp = -\partial\Psi/\partial r = 0$) and at $r \to \infty$ (B finite), we obtain

$$\Psi(r,\theta) = A_1\left(r + \frac{a^2}{r}\right)e^{i\theta} + \text{c.c.} \qquad (4)$$

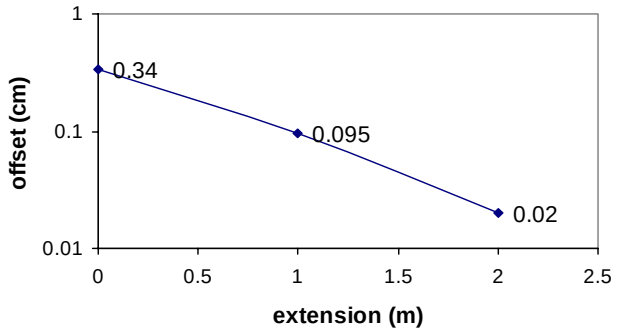

FIG. 7. (Color) Transverse offset of beam centroid 40 cm from cathode as a function of added cathode stalk length (beam current ≈4.8 kA).

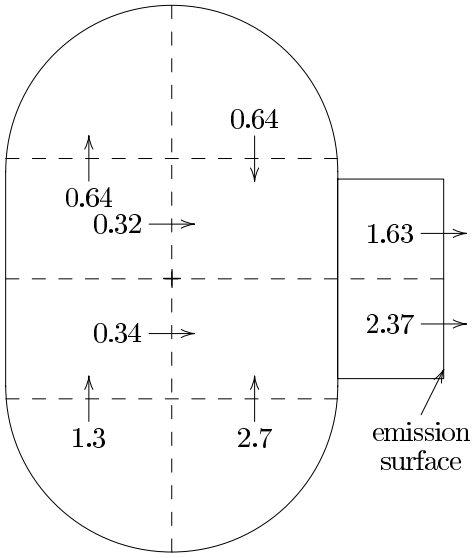

FIG. 8. Coarse-grained diagram of current flow in the cathode dome (units of kA). The emission surface is on the right.

The dipole current is then given by

$$I_d = \frac{1}{\mu_0}\int_0^{\pi} B_\theta dl = \frac{4B_0 a}{\mu_0}, \qquad (5)$$

where B_0 is the transverse magnetic field as $r \to \infty$. Inserting the values for the stalk in Fig. 1, i.e., $a = 0.4$ m, $B_0 \approx 3 \times 10^{-4}$ T (3 G), we get $I_d \approx 380$ A. This is in reasonable agreement with the simulation value ($740/2 = 370$ A).

The electric field asymmetry in the AK gap is considerably smaller than the magnetic field asymmetry: The simulations show that the transverse electric force in the AK gap is about 50 times smaller than the transverse magnetic force. As a corollary to this, we expect the beam emitted from the cathode to be symmetric to a high degree. Thus the asymmetric currents flowing in the cathode stalk rearrange themselves on the emitting face to produce an (almost) symmetric beam. There may be some higher-pole magnetic fields associated with this process, but we have not yet attempted to calculate them. A finer grid than we are using here would be needed to accurately compute these fields as well as the asymmetry in the emitted current density.

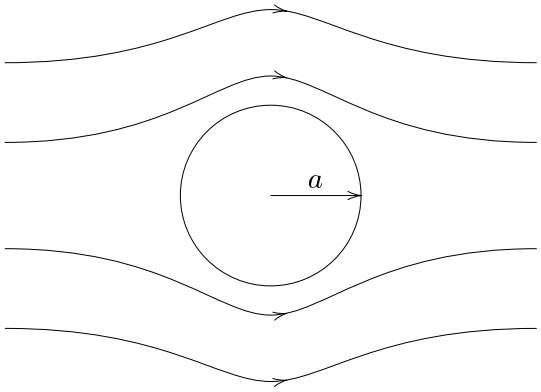

FIG. 9. Geometry for calculation of dipole current in a conducting cylinder immersed in a transverse magnetic field. The radius of the cylinder (representing the cathode stalk) is a.

III. rf PERTURBATIONS

The LSP calculations reveal that, in addition to a quasistatic deflection, the beam centroid undergoes small-amplitude transverse oscillations. The beam displacement 40 cm from the cathode surface is shown on a magnified scale in Fig. 10. The frequency spectrum shows peaks at 38, 54, and 78 MHz. By externally driving the injector cavity at each of these frequencies to establish the mode patterns, we find that they are predominantly TE_{11}-like modes of the vacuum vessel. The dispersion relation for TE_{11} modes in a cylindrical cavity of length L, radius b with a center conductor of radius a is

$$J_1'(a\gamma)Y_1'(b\gamma) - Y_1'(a\gamma)J_1'(b\gamma) = 0, \qquad (6)$$

where $\gamma = \sqrt{\omega^2/c^2 - k_z^2}$ and $k_z = (2n-1)\pi/L$, $n = 1, 2, \ldots$ is the axial wave number. For $a = 0.5$ m (the radius of the 5 kΩ resistor), $b = 2$ m, $L = 8$ m, the lowest frequency is about 44 MHz. In the actual geometry, this is lowered to 38 MHz (see Fig. 10), probably by the AK gap structure. The frequencies in Fig. 10 are in rough agreement with frequency-domain calculations using the MAFIA code and a LANL finite-element code [3].

The amplitude of the transverse oscillations is significantly affected by the 5 kΩ resistor and by the oil ($\epsilon = 2.3$) dielectric (see Fig. 1). In Fig. 11, we show the larger amplitudes obtained when the resistor is removed, and when both the resistor and the oil are removed (by setting $\epsilon = 1$ in the oil region). A separate simulation

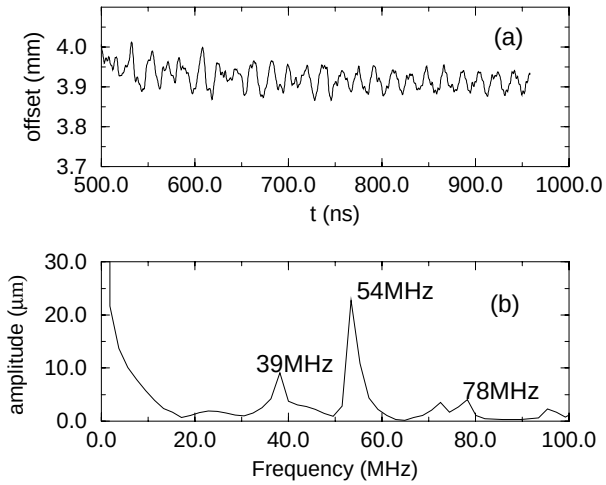

FIG. 10. Beam transverse displacement vs time is plotted on a magnified scale in (a). The Fourier transform is shown in (b).

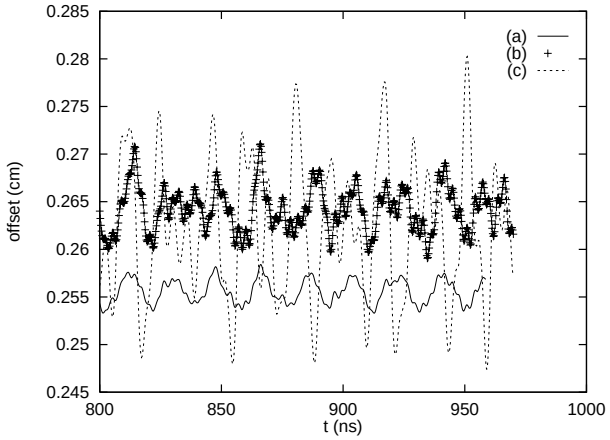

FIG. 11. Comparison of transverse oscillations for (a) 5 kΩ resistor, $\epsilon = 2.3$ oil; (b) no resistor, $\epsilon = 2.3$ oil; (c) no resistor and $\epsilon = 1$ oil.

shows an amplitude drop of 20% in going from a 7 kΩ to a 5 kΩ resistor.

Since the amplitude of the transverse oscillations is about the same magnitude as the design specification for beam alignment (100 μm), schemes for damping the rf modes have been modeled numerically. In one scheme, we placed a ring of ferrite material 50 cm high and 3 cm thick around the inside wall of the vacuum vessel near the bottom, where the magnetic field of the TE_{11} modes has an antinode. The effect was modeled using the dispersive-material model in LSP, with a single relaxation pole of the form

$$\mu(\omega) = \mu_\infty + \frac{\mu_s - \mu_\infty}{1 + i\omega/\delta}, \tag{7}$$

where μ_∞, μ_s, and δ were chosen to match the real and imaginary permeability values for "ETA-II ferrite" in the region of 50 MHz ($\mu_r \approx 50$, $\mu_i \approx 100$) as given in

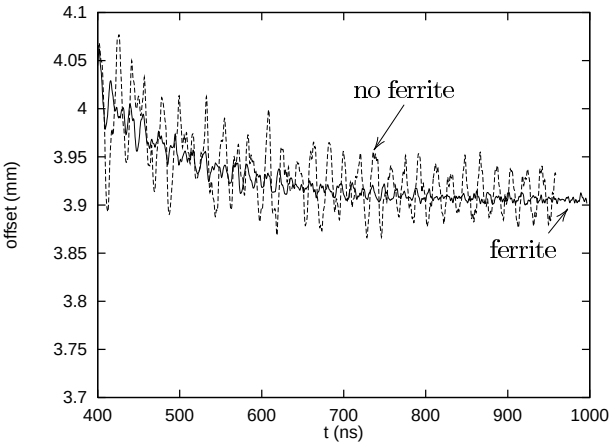

FIG. 12. Comparison of beam centroid motion with and without ferrite-ring damper.

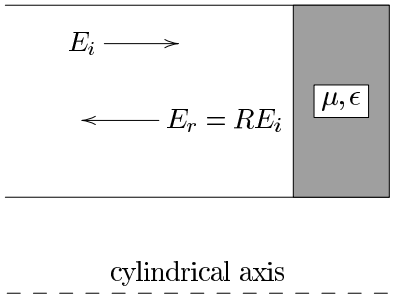

FIG. 13. Coaxial geometry for calculation of the ferrite reflection coefficient.

Ref. [4]. The numerical results show a strong damping of the rf-driven centroid oscillations to below 20 μm, as shown in Fig. 12. In the simulation, the thickness of the ferrite ring cannot be made smaller than the radial cell size (3 cm). Thinner ferrite may have a larger damping effect, however. In the coaxial geometry shown in Fig. 13, which is like that used in Ref. [4] to measure the ferrite properties, the reflection coefficient of a ferrite toroid is calculated to be

$$R = \frac{1 - e^{2ik\Delta} - \sqrt{\epsilon/\mu}\,(1 + e^{2ik\Delta})}{1 - e^{2ik\Delta} + \sqrt{\epsilon/\mu}\,(1 + e^{2ik\Delta})}, \tag{8}$$

where Δ is the ferrite thickness and k is the axial wave number. In Fig. 14 we see that the optimal thickness for frequencies in the range 40–70 MHz is on the order of 1 cm. The enhanced absorption is due to reflection of the incident wave from the conducting surface behind the ferrite. We have verified that the dispersive-material model in LSP agrees with Eq. (8).

IV. CONCLUSIONS

The asymmetric design of the DARHT-2 injector produces both quasistatic and rf transverse displacements of the beam centroid. We have modeled these effects with the 3D electromagnetic particle-in-cell code LSP. For a 4 kA beam current, the quasistatic transverse magnetic field is on the order of 3–4 G and produces a beam deflection of several millimeters at the anode. The effect will be corrected using static magnetic dipoles. The rf oscillations are produced by TE_{11}-like modes of the injector

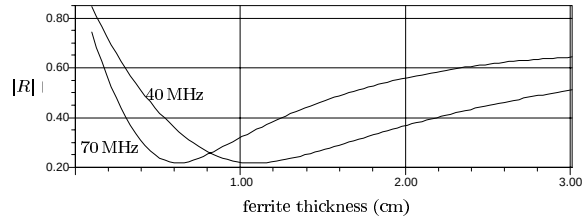

FIG. 14. Reflection coefficient of ferrite vs thickness for two incident frequencies.

vessel excited by the current rise. Using ferrite damping, the oscillation amplitude can be reduced to <20 μm. The DARHT-2 injector will be operated initially at 2 kA, which further reduces the deflection amplitudes by a factor of 2.

ACKNOWLEDGMENTS

We thank Bill Fawley, Enrique Henestroza, Eric Nelson, and Dan Prono for useful discussions. Figure 3 was created using the GMV graphics postprocessor of Frank Ortega (LANL). This work was supported by Los Alamos National Laboratory.

[1] M. J. Burns, B. E. Carlsten, T. J. T. Kwan, D. C. Moir, D. S. Prono, S. A. Watson, E. L. Burgess, H. L. Rutkowski, G. J. Caporaso, and Y.-J. Chen, in Proceedings of the 1999 Particle Accelerator Conference (PAC99), New York (to be published) (http://ftp.pac99.bnl.gov/Papers/Wpac/FRAR4.pdf).

[2] LSP is a product of Mission Research Corp., Albuquerque, NM.

[3] Enrique Henestroza and Eric Nelson (private communications).

[4] J. F. DeFord and G. Kamin, in *Proceedings of the 1990 Linear Accelerator Conference, Albuquerque, New Mexico* (Los Alamos National Laboratory, Los Alamos, NM, 1991), p. 384.